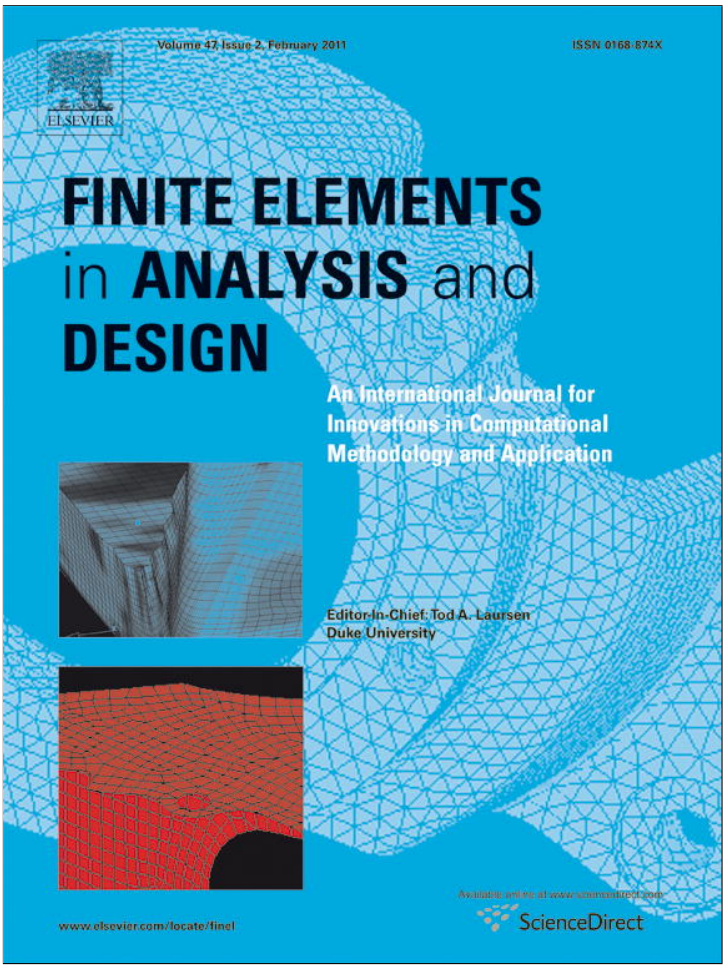

(This is a sample cover image for this issue. The actual cover is not yet available at this time.)

Finite Elements in Analysis and Design 52 (2012) 31–40

Contents lists available at SciVerse ScienceDirect

Finite Elements in Analysis and Design

journal homepage: www.elsevier.com/locate/finel

Analytic and finite element solutions of the power-law Euler–Bernoulli beams

Dongming Wei [a,*], Yu Liu [b,**]

[a] Mathematics Department, University of New Orleans, 2000 Lakeshore Dr. New Orleans, LA 70148, USA
[b] Electrical Engineering Department, University of New Orleans, 2000 Lakeshore Dr. New Orleans, LA 70148, USA

ARTICLE INFO

Article history:
Received 30 January 2011
Received in revised form
11 September 2011
Accepted 20 December 2011

Keywords:
Finite element solution
Ritz–Galerkin method
Nonlinear Euler–Bernoulli beam
Power-law
Work hardening material
Hollomon's equation
Convergence
Error estimate
Hermite elements

ABSTRACT

In this paper, we use Hermite cubic finite elements to approximate the solutions of a nonlinear Euler–Bernoulli beam equation. The equation is derived from Hollomon's generalized Hooke's law for work hardening materials with the assumptions of the Euler–Bernoulli beam theory. The Ritz–Galerkin finite element procedure is used to form a finite dimensional nonlinear program problem, and a nonlinear conjugate gradient scheme is implemented to find the minimizer of the Lagrangian. Convergence of the finite element approximations is analyzed and some error estimates are presented. A Matlab finite element code is developed to provide numerical solutions to the beam equation. Some analytic solutions are derived to validate the numerical solutions. To our knowledge, the numerical solutions as well as the analytic solutions are not available in the literature.

Published by Elsevier B.V.

1. Introduction

The following power-law is frequently used to model axial stress-strain relations for annealed metals:

$$\sigma = K|\varepsilon|^{n-1}\varepsilon$$

where σ is the stress, ε is the strain, and K and n are constant. Materials modeled by the above power-law equation are called work-hardening materials, sometimes referred to as Hollomon or Ludwick materials. The values of K and n for some common annealed metals can be found in undergraduate textbooks and in engineering literature, e.g., see [1–3]. Modern applications of these work-hardening metals can be found from bumper beams in the automobile industry [4] to micro-grippers in bio-engineering [5].

These materials and the power-law equation are widely introduced to undergraduate engineering students at the sophomore level. More sophisticated beam equations that model the power-law materials exist but are less accessible to the students, see, e.g., [6–8]. However, to our knowledge, there are very few mathematical models in the literature which provide simple bench mark analytic or numerical solutions for modeling mechanical structures made of these materials.

In this work, we study the following nonlinear beam equation for the power-law materials:

$$\frac{d^2}{dx^2}\left(KI_n\left|\frac{d^2v}{dx^2}\right|^{n-1}\frac{d^2v}{dx^2}\right)-f(x)=0,\quad 0<x<L \tag{1}$$

where $v(x)$ is the transversal deflection of the beam, x is the axial location, I_n (where $n\neq 1$) is the generalized moment of inertia.

For the case $n=1$, this equation reduces to the standard Euler–Bernoulli equation for an elastic beam, which has been studied extensively. For a good account of finite element solutions for this case, see [9]. Further, Reddy [10] examined nonlinear versions of elastic Euler–Bernoulli beams (which are more general than linear case) and their finite element solutions.

Several authors have studied the following similar beam equation:

$$nK\left(\frac{d\phi}{ds}\right)^{n-1}\frac{d^2\phi}{ds^2}-P\sin(\phi+\alpha)=0,\quad 0<s<L \tag{2}$$

for the power-law materials, where s is the arc length, ϕ is the bending angle at s, P is the end load applied with an angle α. The paper by Kang and Li [7] provides a solution of Eq. (2) for a punctual load at $s=L$ (the end). Their solution coincides with our

* Principal corresponding author. Tel.: +1 504 280 6123; fax: +1 504 280 5516.
** Corresponding author. Tel.: +1 504 261 1126.
E-mail addresses: dwei@uno.edu (D. Wei), lyu2@uno.edu (Y. Liu).

0168-874X/$ - see front matter Published by Elsevier B.V.
doi:10.1016/j.finel.2011.12.007

Nomenclature

$\overline{x}$	the local coordinates
$\mathbf{V}$	the set of all the possible displacements which give finite energy and subject to a set of appropriate essential boundary conditions
$\chi^{(e)}(x)$	the characteristic (or indicator) function
$\{c_1,c_2,c_3,c_4\}$	the integration constants to be determined by the boundary conditions
$\mathbf{1}(x)$	the unit step function
$\phi_i^{(e)}$	the ith local finite element shape function for the eth element interval
σ	the stress
$\delta(x)$	Dirac delta function
ε	the strain
A	the cross sectional area of the beam
C	the connectivity matrix
e	the index of the element
F	the magnitude of the punctual load
$f(x)$	the vertical distributed load
I_n	the generalized moment of inertia
$I(\mathbf{u})$	Lagrangian energy functional
K,v	material constants
$l^{(e)}$	the length of the eth subinterval
ne	total number of subintervals on x
n_L	the number of local shape functions
v	the vector of global nodal values
$v(x)$	the vertical displacement of the beam at location x
$V(x)$	the global Hermite cubic interpolation function
$V^{(e)}(x)$	local interpolation function
$v_i^{(e)}$	the ith local nodal value
x	the global coordinates
x_F	the location of the punctual load
GQ	Gaussian quadrature
NCG	Nonlinear conjugate gradient

solution when $\alpha=\pi/2$. Large deflections of the beam are also studied by them. Teng and Wierzbicki [11] derived analytic solutions and numerical solutions of Eq. (2) for a power-law beam subject to a punctual load at one end. The Timoshenko beam element in Abacus was used by them to obtain numerical solutions for comparison with the analytic solutions.

Further, the more recent work of [8] that gives an analytical solution in couple stress elasto-plastic theory is presented for the pure bending beam under small deformation.

There are many papers devoted to the study of the Euler–Bernoulli beam for functionally graded materials with thickness dependent material constants, for small and large deflections, see Yahoobi and Feraidoon [12] and the references therein. Wang, et al. [6] study large deformation of functionally graded cantilever beams for the power-law material, both experimentally and analytically.

In this work, we use the Ritz–Galerkin's finite element method to approximate the solutions of the power-law Euler–Bernoulli beam equation. Hermite cubic finite elements and the nonlinear conjugate gradient scheme (NCG) [13] are used in the Ritz–Galerkin finite element method for solutions of the beam equation. A finite element code in Matlab is written to implement the numerical scheme and to provide numerical solutions. Analytic solutions including two special cases to the beam equation are derived for validation of the numerical solutions. It is shown that the numerical solutions compare favorably with the analytic solutions. We also provide convergence analysis and error estimates. To our knowledge, these numerical solutions as well as the analytic solutions are not available in the literature.

2. The power-law Euler–Bernoulli beam equation

A general form of the Hollomon equation can be written as [14]:

$$\begin{bmatrix}\sigma_x\\ \sigma_y\\ \sigma_z\\ \tau_{xy}\\ \tau_{yz}\\ \tau_{zx}\end{bmatrix}=C\begin{bmatrix}1-v & v & v & 0 & 0 & 0\\ v & 1-v & v & 0 & 0 & 0\\ v & v & 1-v & 0 & 0 & 0\\ 0 & 0 & 0 & 1-2v & 0 & 0\\ 0 & 0 & 0 & 0 & 1-2v & 0\\ 0 & 0 & 0 & 0 & 0 & 1-2v\end{bmatrix}\begin{bmatrix}\epsilon_x\\ \epsilon_y\\ \epsilon_z\\ \gamma_{xy}\\ \gamma_{yz}\\ \gamma_{zx}\end{bmatrix} \tag{3}$$

where

$$C=\frac{K|D(\mathbf{u})|^{n-1}}{(1+v)(1-2v)}$$

$$D(\mathbf{u})=\begin{bmatrix}\epsilon_x & \gamma_{xy} & \gamma_{xz}\\ \gamma_{yx} & \epsilon_y & \gamma_{yz}\\ \gamma_{zx} & \gamma_{zy} & \epsilon_z\end{bmatrix}$$

$$|D(\mathbf{u})|=\sqrt{\epsilon_x^2+\epsilon_y^2++\epsilon_z^2+2\gamma_{xy}^2+2\gamma_{yz}^2+2\gamma_{zx}^2}$$

with K and v are material constants. When $n=1$, K equals the Young's modulus of linear elasticity and v the corresponding Poisson's ratio. Note that some notations, e.g., C, may be used for multiple meanings later. It should incur no ambiguity within the context. The Lagrangian energy functional $I(\mathbf{u})$ for a power-law elastoplastic body occupying a three dimension body V can be defined by the kinetic energy minus the elastoplastic potential energy plus the work done by external forces. It can be written as:

$$I(\mathbf{u})=\frac{1}{2}\int_V\rho\dot{\mathbf{u}}\dot{\mathbf{u}}^\tau\,dV-\frac{1}{n+1}\int_V\sigma\epsilon^\tau\,dV+\int_V\mathbf{f}\mathbf{u}^\tau\,dV+\int_{\partial V}\mathbf{t}\mathbf{u}^\tau \tag{4}$$

where $\boldsymbol{\epsilon}=(\epsilon_x,\epsilon_y,\epsilon_z,\gamma_{xy},\gamma_{xz},\gamma_{yz})$, and $\boldsymbol{\sigma}=(\sigma_x,\sigma_y,\sigma_z,\tau_{xy},\tau_{xz},\tau_{yz})$, ρ is the density, $\dot{\mathbf{u}}=(\dot{u},\dot{v},\dot{w})$ the velocity, $\mathbf{f}=(f_x,f_y,f_z)$ the body force, and $\mathbf{t}=(t_x,t_y,t_z)$ the surface force. For the power-law Euler–Bernoulli beam, it is assumed that the components of the displacement satisfy

$$\begin{cases}u=-y\dfrac{\partial v}{\partial x}\\ v=v(x,t)\\ w=0\\ \mathbf{f}=(0,r(x,t),0)\\ \mathbf{t}=(0,0,0)\end{cases}$$

Therefore

$$\begin{cases}\epsilon_x=\dfrac{\partial u}{\partial x}=-y\dfrac{\partial^2 v}{\partial x^2}\\ \epsilon_{xy}=\dfrac{1}{2}\left(\dfrac{\partial u}{\partial y}+\dfrac{\partial v}{\partial x}\right)=0\\ \epsilon_y=\epsilon_{xz}=\epsilon_{yz}=\epsilon_z=0\end{cases}$$

The Lagrangian for the beam is given by

$$I(v)=\frac{1}{2}\int_0^L \rho_0\dot{v}^2+\frac{1}{n+1}\int_0^L KI_n\left|\frac{\partial^2 v}{\partial x^2}\right|^{n+1}dx-\int_0^L f(x)v(x)\,dx \tag{5}$$

where $I_n=\int_A|y|^{n+1}\,dy\,dz$ is the generalized moment of inertia of the beam. The following forth-order beam equation can be derived by the principle of virtual work:

$$\rho_0\frac{\partial^2 v}{\partial t^2}-\frac{\partial^2}{\partial x^2}\left(KI_n\left|\frac{\partial^2 v}{dx^2}\right|^{n-1}\frac{\partial^2 v}{\partial x^2}\right)-f(x)=0,\quad 0<x<L \tag{6}$$

where $v(x)$ is the vertical displacement of the beam at the axial location x; $f(x)$ is the vertical load; A is the cross sectional area of the beam; See [14] for details of the derivation of (6), which is referred to as the power-law Euler–Bernoulli beam equation in this paper, and we only consider analytic and numerical solutions of the corresponding steady state, i.e., Eq. (1).

3. The Ritz variational principle

It is known that the Euler–Lagrange equation for a Lagrangian functional of the general form:

$$I(v)=\int_a^b G(x,v(x),v'(x),v''(x))\,dx$$

is

$$\frac{d^2}{dx^2}\left(\frac{\partial G}{\partial v''}\right)-\frac{d}{dx}\left(\frac{\partial G}{\partial v'}\right)+\frac{\partial G}{\partial v}=0,\quad a<x<b$$

The corresponding natural boundary conditions and essential boundary conditions are

$$\frac{d}{dx}\left(\frac{\partial G}{\partial v''}\right)-\frac{\partial G}{\partial v'}=0,\frac{\partial G}{\partial v''}=0,\quad \text{for } x=a \text{ or } x=b$$

and

$$v(a)=A,v'(a)=B,v(b)=C,v'(b)=D$$

respectively. The Euler–Lagrange equation requires four boundary conditions in order to have a unique solution. For details, see [15]. In particular, for the steady state power-law Euler–Bernoulli beam, we have

$$G(x,v'(x),v''(x))=\frac{KI_n}{n+1}|v''|^{n+1}-fv$$

and the corresponding Euler–Lagrange equation:

$$\frac{\partial^2}{\partial x^2}\left(KI_n\left|\frac{\partial^2 v}{dx^2}\right|^{n-1}\frac{\partial^2 v}{\partial x^2}\right)-f(x)=0,\quad 0<x<L \tag{7}$$

with natural boundary conditions

$$KI_n|v''|^{n-1}v'''=0\quad \text{or } KI_n|v''|^{n-1}v''=0$$

at $x=a$ or $x=b$. The Ritz variational principle states that $v(x)$ represents the displacement of the beam at equilibrium subject to appropriate boundary conditions if and only if $v(x)$ is the solution of the following minimization problem:

$$\min I(v)\quad \text{s.t. } v\in\mathbf{V} \tag{8}$$

where $\mathbf{V}$ is the set of all the possible displacements which give finite energy and are subjected to a set of appropriate essential boundary conditions.

The exact solution v(x) of Eq. (7) can be approximated by the standard finite element approximation:

$$V^{(e)}(x)=\sum_{i=1}^{n_L}\phi_i^{(e)}(x)v_i^{(e)}=\boldsymbol{\phi}^{(e)T}\mathbf{v}^{(e)},\quad x_1^{(e)}<x<x_2^{(e)} \tag{9}$$

where $\phi_i^{(e)}$ is the ith local finite element shape function defined in the eth interval $x_1^{(e)}<x<x_2^{(e)}$; $v_i^{(e)}$ is the ith local nodal value associated with the exact solution at $x_i^{(e)}$; denote $\mathbf{v}^{(e)}=[v_1^{(e)}\ v_2^{(e)}\ \cdots\ v_{n_L}^{(e)}]^T$ and $\boldsymbol{\phi}^{(e)}=[\phi_1^{(e)}\ \phi_2^{(e)}\ \cdots\ \phi_{n_L}^{(e)}]^T$; e is the index of the element; n_L is the number of local shape functions.

A natural choice of the shape functions for our problem is the Hermite cubic shape functions [9], which are defined as:

$$\phi_1^{(e)}=1-3\left(\frac{\bar{x}}{l^{(e)}}\right)^2+2\left(\frac{\bar{x}}{l^{(e)}}\right)^3,\quad \phi_2^{(e)}=-\bar{x}\left(1-\frac{\bar{x}}{l^{(e)}}\right)^2$$

$$\phi_3^{(e)}=3\left(\frac{\bar{x}}{l^{(e)}}\right)^2-2\left(\frac{\bar{x}}{l^{(e)}}\right)^3,\quad \phi_4^{(e)}=-\bar{x}\left[\left(\frac{\bar{x}}{l^{(e)}}\right)^2-\left(\frac{\bar{x}}{l^{(e)}}\right)\right]$$

and the corresponding second derivatives which will be used latter are also given below:

$$\frac{d^2\phi_1^{(e)}}{d\bar{x}^2}=-\frac{6}{[l^{(e)}]^2}\left(1-\frac{2\bar{x}}{l^{(e)}}\right),\quad \frac{d^2\phi_2^{(e)}}{d\bar{x}^2}=-\frac{2}{l^{(e)}}\left(\frac{3\bar{x}}{l^{(e)}}-2\right)$$

$$\frac{d^2\phi_3^{(e)}}{d\bar{x}^2}=\frac{6}{[l^{(e)}]^2}\left(1-\frac{2\bar{x}}{l^{(e)}}\right),\quad \frac{d^2\phi_4^{(e)}}{d\bar{x}^2}=-\frac{2}{l^{(e)}}\left(\frac{3\bar{x}}{l^{(e)}}-1\right)$$

where $\bar{x}=x-x_1^{(e)}$ is the local coordinates; $l^{(e)}=x_2^{(e)}-x_1^{(e)}$ is the length of the eth subinterval.

Let ne denote the total number of subintervals on x. In the Ritz–Galerkin method, we look for the solution by minimizing the following energy function:

$$I(V)=\sum_{e=1}^{ne}I^{(e)}(V^{(e)})$$

where

$$I^{(e)}(V^{(e)})=\frac{1}{n+1}\int_{x_1^{(e)}}^{x_2^{(e)}}KI_n\left|\frac{d^2V^{(e)}}{dx^2}\right|^{n+1}dx-\int_{x_1^{(e)}}^{x_2^{(e)}}f(x)V^{(e)}\,dx$$

and $V(x)=\sum_{e=1}^{ne}\chi^{(e)}V^{(e)}(x)$ is global Hermite cubic interpolation function, $V^{(e)}(x)$ is given in Eq. (9);

$$\chi^{(e)}(x)=\begin{cases}1 & \text{if } x\in[x_1^{(e)},x_2^{(e)}]\\ 0 & \text{if } x\notin[x_1^{(e)},x_2^{(e)}]\end{cases}$$

is the characteristic (or indicator) function.

Denote $\mathbf{v}=[v_1\ v_2\ \cdots\ v_{2ne+2}]^T$ as the global nodal values, then the connections between the global nodal values and local nodal values are

$$v_{2e-1}=v_1^{(e)},\quad v_{2e}=v_2^{(e)}$$

$$v_{2e+1}=v_3^{(e)},\quad v_{2(e+1)}=v_4^{(e)}\quad \text{for } e=1,\ldots,ne.$$

So the eth row of the $2(ne+1)\times 4$ connectivity matrix C can be defined by

$$[c_{e,1},c_{e,2},c_{e,3},c_{e,4}]=[2e-1,2e,2e+1,2e+2],\quad \text{for } e=1,2,\ldots,ne.$$

It can be shown that $I(V)$ is convex function of $\mathbf{v}$ and has a unique global minimum at which the gradient ∇I must equal 0, i.e., $\partial I/\partial\mathbf{v}=0$. The gradient of the local element energy function $I^{(e)}$ relative to the local degrees of freedom $\mathbf{v}^{(e)}=[v_1^{(e)},\ v_2^{(e)},\ v_3^{(e)},\ v_4^{(e)}]^T$ is

$$\frac{\partial I^{(e)}}{\partial\mathbf{v}^{(e)}}=\left[\frac{\partial I^{(e)}}{\partial v_1^{(e)}},\frac{\partial I^{(e)}}{\partial v_2^{(e)}},\frac{\partial I^{(e)}}{\partial v_3^{(e)}},\frac{\partial I^{(e)}}{\partial v_4^{(e)}}\right]^T$$

$$=\frac{1}{n+1}\int_{x_1^{(e)}}^{x_2^{(e)}}KI_n\left(\frac{\partial}{\partial\mathbf{v}^{(e)}}\left|\frac{d^2V^{(e)}}{dx^2}\right|^{n+1}\right)dx-\int_{x_1^{(e)}}^{x_2^{(e)}}f(x)\frac{\partial V^{(e)}}{\partial\mathbf{v}^{(e)}}dx \tag{10}$$

Since $V^{(e)}=\boldsymbol{\phi}^{(e)T}\mathbf{v}^{(e)}$ and $d^2V^{(e)}/dx^2=(d^2\boldsymbol{\phi}^{(e)T}/dx^2)\mathbf{v}^{(e)}$, we have

$$\frac{\partial V^{(e)}}{\partial \mathbf{v}^{(e)}}=\boldsymbol{\phi}^{(e)},\quad \frac{\partial}{\partial \mathbf{v}^{(e)}}\left(\frac{d^2V^{(e)}}{dx^2}\right)=\frac{d^2\boldsymbol{\phi}^{(e)}}{dx^2}$$

and

$$\begin{aligned}\frac{\partial}{\partial \mathbf{v}^{(e)}}\left|\frac{d^2V^{(e)}}{dx^2}\right|^{n+1}&=(n+1)\left|\frac{d^2V^{(e)}}{dx^2}\right|^{n-1}\left(\frac{d^2V^{(e)}}{dx^2}\right)\frac{\partial}{\partial \mathbf{v}^{(e)}}\left(\frac{d^2V^{(e)}}{dx^2}\right)\\&=(n+1)\left|\frac{d^2V^{(e)}}{dx^2}\right|^{n-1}\left(\frac{d^2V^{(e)}}{dx^2}\right)\frac{d^2\boldsymbol{\phi}^{(e)}}{dx^2}\end{aligned}\tag{11}$$

Substituting Eq. (11) into Eq. (10), it yields

$$\frac{\partial I^{(e)}}{\partial \mathbf{v}^{(e)}}=\int_{x_1^{(e)}}^{x_2^{(e)}}KI_n\left|\frac{d^2V^{(e)}}{dx^2}\right|^{n-1}\left(\frac{d^2V^{(e)}}{dx^2}\right)\frac{d^2\boldsymbol{\phi}^{(e)}}{dx^2}dx-\int_{x_1^{(e)}}^{x_2^{(e)}}f(x)\boldsymbol{\phi}^{(e)}\,dx\tag{12}$$

So the gradient of the global energy function is

$$\frac{\partial I}{\partial \mathbf{v}}=\left[\frac{\partial I}{\partial v_1},\frac{\partial I}{\partial v_2},\ldots,\frac{\partial I}{\partial v_{2(ne+1)}}\right]^T$$

where

$$\frac{\partial I}{\partial v_j}=\sum_{e=1}^{ne}\sum_{c_{(e,i)}=j}\frac{\partial I^{(e)}}{\partial v_i^{(e)}}$$

The summation $\sum_{e=1}^{ne}\sum_{c_{(e,i)}=j}$ is performed over all elements with local nodes that share the global node number j. In the process of evaluating the integral in Eq. (12), numerical overflow may arise for $0<n<1$ and for small values of the term $|d^2V^{(e)}/dx^2|$, since the term $|d^2V^{(e)}/dx^2|^{n-1}$ may take on very large values and lead to divergence. One simple remedy to this problem is to evaluate the term in the following way:

$$\left|\frac{d^2V^{(e)}}{dx^2}\right|^{n-1}\left(\frac{d^2V^{(e)}}{dx^2}\right)=\begin{cases}\left(\dfrac{d^2V^{(e)}}{dx^2}\right)^n & \text{if } \dfrac{d^2V^{(e)}}{dx^2}\geq 0\\ -\left|\dfrac{d^2V^{(e)}}{dx^2}\right|^n & \text{if } \dfrac{d^2V^{(e)}}{dx^2}<0\end{cases}$$

In order to evaluate the integrals in $I^{(e)}$ and $\nabla I^{(e)}$, numerical integration, such as Gaussian quadrature (GQ), can be performed. The GQ is a quadrature rule to yield an exact solution for polynomials of degree $2n_Q-1$ or less by a suitable choice of the points x_i and weights ω_i, where n_Q is the number of the points chosen for the quadrature. A detailed table for the values of ω_i and x_i can be found in [16].

4. Convergence of the finite element approximations

Let $\phi(x)=|x|^{r-2}x$, then the following inequalities:

$$|x-y|^2\leq C(\phi(x)-\phi(y),x-y)(|x|+|y|)^{2-r}\tag{13}$$

$$|\phi(x)-\phi(y)|\leq C|x-y|^{r-1}\quad \text{for } 1<r<2\tag{14}$$

hold for all $x, y\in R^m$, where $m\geq 1$, (x,y) denotes the inner product; the constant $C>0$ is independent of x and y. A simple proof of the above inequalities is shown in [17,18]. The convergence and error analysis of our problem is based on the Aubin-Nitsche trick and the above inequalities. Let $r=n+1$, let $W_b^{2,r}(0,L)$ be the space defined by the set of admissible functions v satisfying $\int_0^L(|v''|^r+|v'|^r+|v|^r)\,dx<\infty$; where $v(0),v(L),v'(0)$, and $v'(L)$ are given, and let $W_0^{2,r}(0,L)$ be the set of admissible functions u with zero boundary conditions, satisfying $\int_0^L(|u''|^r+|v'|^r+|u|^r)\,dx<\infty$, the corresponding $u(0),u(L),u'(0)$, and $u'(L)$ are zero. Then, the problem of finding the minimizer v of the energy functional $I(v)$ for the solution of our beam equation can be written as the following variational equivalent problem:

Problem (P_0). Find $v\in W_b^{2,r}(0,L)$, such that for all $u\in W_0^{2,r}(0,L)$,

$$a(v,u)=\langle f,u\rangle$$

where $a(v,u)=\int_0^L KI_n|\partial^2v/dx^2|^{n-1}(\partial^2v/\partial x^2,\partial^2u/\partial x^2)\,dx$, and $\langle f,u\rangle=\int_0^L fu\,dx$.

If $S_{b,h}^{2,r}(0,L)$ denotes the set of global Hermite cubic finite element interpolation functions as a conformal subspace of $W_b^{2,r}(0,L)$, then the minimizer U_h of $I(U)$ over the set $S_{b,h}^{2,r}(0,L)$ is the unique solution of the following problem:

Problem (P_h). Find $U_h\in S_{b,h}^{2,r}(0,L)$, such that for all $U\in S_{0,h}^{2,r}(0,L)$:

$$a(U_h,U)=\langle f,U\rangle$$

where $a(U_h,U)=\int_0^L KI_n|\partial^2U_h/dx^2|^{n-1}(\partial^2U_h/\partial x^2,\partial^2U/\partial x^2)\,dx$, and $\langle f,U\rangle=\int_0^L fU\,dx$. By the Aubin-Nitsche trick and the above inequalities, we have the following error estimate:

Theorem. *Let v be the exact solution of (P_0) and let U_h be the finite element solution of (P_h), let $h=max_{1\leq i\leq N}\Delta x_i$ be the maximum finite element mesh size, then*

$$\|v-U_h\|\leq Ch^{1/(3-r)}\tag{15}$$

where $\|v-U_h\|=(\int_0^L|v''(x)-U_h''(x)|^r\,dx)^{1/r}$, and C is a generic constant independent of h.

The proof is omitted here since it similar to the classical work of Glowinski and Morrocco [18]. Similar optimal error estimates can be obtained by the work of Barrett and Liu [19]. Since $r=n+1$, the order of convergence is $O(h^{1/(2-n)})$. It equals $O(h)$ when $n=1$ and $O(h^{1/2})$ when $n\to 0$. This partially explains that convergence is slower, in our numerical examples, for values of n closer to zero. For the optimization problem (Eq. (8)) in this work, many nonlinear optimization techniques [20], e.g., nonlinear conjugate gradient (NCG), Newton–Raphson, interior-point or active-set method, are applicable. We implemented NCG simply for its good combination among the simplicity, the convergence rate and computational efficiency. Further, only the gradient of the objective function is involved in NCG method, rendering it numerically more robust than methods requiring Hessian matrix (e.g., Newton–Raphson method). Slight modifications are made to accommodate the constraints. Note, If let $J(x)=I(V)$, in which $x=[v_1,v_2,\ldots,v_{2ne+2}]^T$, even though ∇J is not a self-adjoint positive definite matrix, it however has the "monotonicity" property, i.e., $\langle\nabla J(x)-\nabla J(y),x-y\rangle\geq C\|x-y\|^2$ for all x,y, by using (14). This inequality provides the sufficient condition for convergence of the NCG iterations. See, e.g., [21] for proof of convergence.

5. Exact solutions for some special cases

We show that in some special cases, analytical solutions of the power-law Euler–Bernoulli Eq. (1) can be derived for $n\neq 1$. Many analytic solutions to the case $n=1$ are classical and we do not elaborate on them. These analytic solutions provide us more insight for the problem solutions and also they can be a performance measure of the finite element solutions. In this section, KI_n is assumed constant w.r.t x.

5.1. Case 1, constant distributed load

If $f(x)$ is constant (w.r.t. x), then Eq. (7) has the following equivalent form:

$$\frac{d^2}{dx^2}\left(\left|\frac{d^2v}{dx^2}\right|^{n-1}\frac{d^2v}{dx^2}\right)=\frac{f}{KI_n},\quad 0<x<L \tag{16}$$

By double integration of Eq. (16), it yields

$$\left|\frac{d^2v}{dx^2}\right|^{n-1}\frac{d^2v}{dx^2}=\frac{f}{2KI_n}x^2+c_1x+c_2 \tag{17}$$

If the beam has a free-end at $x=L$, i.e.,

$$\left.\frac{d^2v}{dx^2}\right|_{x=L}=0,\quad \left.\frac{d^3v}{dx^3}\right|_{x=L}=0 \tag{18}$$

Then the unknown constant c_1 and c_2 in Eq. (17) can be determined. Taking derivative of Eq. (17), we get

$$\left.\frac{d}{dx}\left(\left|\frac{d^2v}{dx^2}\right|^{n-1}\frac{d^2v}{dx^2}\right)\right|_{x=L}=n\left|\frac{d^2v}{dx^2}\right|^{n-1}\left.\frac{d^3v}{dx^3}\right|_{x=L}=\frac{fL}{KI_n}+c_1=0$$

hence $c_1=-fL/KI_n$ and correspondingly $c_2=fL^2/2KI_n$. Therefore, Eq. (17) can be written in the form of complete squares:

$$\left|\frac{d^2v}{dx^2}\right|^{n-1}\frac{d^2v}{dx^2}=\left(\frac{f}{2KI_n}\right)\left(x^2-2Lx+L^2\right)=\left(\frac{f}{2KI_n}\right)(L-x)^2 \tag{19}$$

Note, Eq. (19) implies $d^2v/dx^2\geq 0$ if $f>0$ (the vice versa, $d^2v/dx^2\leq 0$ if $f<0$, the derivations to the solutions are similar for these two cases). So the analytical solution $v(x)$ can be derived:

$$\frac{d^2v}{dx^2}=\left(\frac{f}{2KI_n}\right)^{1/n}(L-x)^{2/n}$$

so

$$v(x)=\frac{\left(\frac{f}{2KI_n}\right)^{1/n}}{\left(\frac{2}{n}+1\right)\left(\frac{2}{n}+2\right)}(L-x)^{2/n+2}+c_3x+c_4$$

where c_3 and c_4 can be determined by the other two boundary conditions, e.g., if the beam is fixed at another end:

$$v(0)=0,\quad \left.\frac{dv}{dx}\right|_{x=0}=0$$

then we have

$$c_3=\frac{\left(\frac{f}{2KI_n}\right)^{1/n}L^{2/n+1}}{\left(\frac{2}{n}+1\right)},\quad c_4=-\frac{\left(\frac{f}{2KI_n}\right)^{1/n}L^{2/n+2}}{\left(\frac{2}{n}+1\right)\left(\frac{2}{n}+2\right)}$$

In general, if different (other than free-end in Eq. (18)) boundary conditions are considered, the complete square form of Eq. (19) can not be obtained, i.e., $c_1^2-2fc_2/KI_n\neq 0$, then the solution becomes much more complicated. Since the function $\lambda(t)=|t|^{n-1}t$ has the inverse function $\lambda^{-1}(t)=|t|^{1/n-1}t$, so the analytical form of d^2v/dx^2 can be derived from Eq. (16):

$$\frac{d^2v}{dx^2}=\left|\frac{f}{2KI_n}x^2+c_1x+c_2\right|^{1/n-1}\left(\frac{f}{2KI_n}x^2+c_1x+c_2\right)$$

If $d^2v/dx^2\geq 0$, then by taking an integral of the above equation, it yields

$$\frac{dv}{dx}=c_3+\frac{2^{1/n}nKI_n}{f(1+n)}\left(c_1-\sqrt{c_1^2-\frac{2fc_2}{KI_n}}+\frac{f}{KI_n}x\right)\times\left(\frac{\sqrt{c_1^2-\frac{2fc_2}{KI_n}}\left(\frac{f}{2KI_n}x^2+c_1x+c_2\right)}{c_1+\sqrt{c_1^2-\frac{2fc_2}{KI_n}}+\frac{f}{KI_n}x}\right)^{1/n}\times\left[{}_2F_1\left(1+\frac{1}{n},-\frac{1}{n},2+\frac{1}{n},\frac{-c_1+\sqrt{c_1^2-\frac{2fc_2}{KI_n}}-\frac{f}{KI_n}x}{2\sqrt{c_1^2-\frac{2fc_2}{KI_n}}}\right)\right]$$

where function ${}_2F_1$ is the well-known Gauss hypergeometric function, see the definition in [22,23]. The constants c_1,c_2,c_3 and the solution $v(x)$ can be obtained by applying the boundary conditions, and using numerical integration of dv/dx.

It is well-known that if $n=1$, the problem becomes linear and much simpler since the term $|dv/dx|^{n-1}$ is gone, then we have

$$\frac{d^4v}{dx^4}=\frac{f}{KI_n},\quad 0<x<L$$

The analytical solution can be easily obtained, that is

$$v(x)=\frac{f}{24KI_n}x^4+c_1x^3+c_2x^2+c_3x+c_4$$

Where the integration constants $\{c_1,c_2,c_3,c_4\}$ can be determined by the boundary conditions.

5.2. Case 2, punctual load

If the punctual load $F\delta(x-x_F)$ is considered, then Eq. (7) has the following form:

$$\frac{d^2}{dx^2}\left(\left|\frac{d^2v}{dx^2}\right|^{n-1}\frac{d^2v}{dx^2}\right)=\frac{F\delta(x-x_F)}{KI_n},\quad 0<x<L$$

where F and x_F are the magnitude and the location ($0<x_F<L$) of the punctual load respectively. Hence

$$\left|\frac{d^2v}{dx^2}\right|^{n-1}\frac{d^2v}{dx^2}=\frac{F\mathbf{1}(x-x_F)}{KI_n}(x-x_F)+c_1x+c_2,\quad 0<x<L$$

where $\mathbf{1}(x-x_F)$ is the unit step function, c_1 and c_2 are determined by boundary conditions, e.g., If the free-end boundary conditions are considered (Eq. (18)), by following the similar idea of case 1, we have

$$\left.\frac{d}{dx}\left(\left|\frac{d^2v}{dx^2}\right|^{n-1}\frac{d^2v}{dx^2}\right)\right|_{x=L}=n\left|\frac{d^2v}{dx^2}\right|^{n-1}\left.\frac{d^3v}{dx^3}\right|_{x=L}=\frac{F}{KI_n}+c_1=0,\quad 0<x<L$$

so $c_1=-F/KI_n$ and correspondingly $c_2=Fx_F/KI_n$. Hence

$$\left|\frac{d^2v}{dx^2}\right|^{n-1}\frac{d^2v}{dx^2}=\frac{F\mathbf{1}(x-x_F)}{KI_n}(x-x_F)-\frac{F}{KI_n}x+\frac{Fx_F}{KI_n}=\frac{F}{KI_n}(x-x_F)[\mathbf{1}(x-x_F)-1],\quad 0<x<L \tag{20}$$

Note, same as the case 1, Eq. (20) implies $d^2v/dx^2\geq 0$ if $F>0$ (vice versa, for $d^2v/dx^2\leq 0$ if $F<0$, the solutions are also similar). Hence, at this case

$$\left(\frac{d^2v}{dx^2}\right)=\left(\frac{F}{KI_n}(x-x_F)[\mathbf{1}(x-x_F)-1]\right)^{1/n},\quad 0<x<L$$

so the exact solution is

$$v(x)=\frac{\left(\frac{F}{KI_n}\right)^{1/n}(x_F-x)^{1/n+2}\mathbf{1}(x_F-x)}{\left(\frac{1}{n}+1\right)\left(\frac{1}{n}+2\right)}+c_3x+c_4,\quad 0<x<L$$

where c_3 and c_4 can be obtained by the other two boundary conditions, e.g., If the beam has another fixed end, then

$$c_3=\frac{\left(\frac{F}{KI_n}\right)^{1/n}x_F^{1/n+1}}{\left(\frac{1}{n}+1\right)},\quad c_4=-\frac{\left(\frac{F}{KI_n}\right)^{1/n}x_F^{1/n+2}}{\left(\frac{1}{n}+1\right)\left(\frac{1}{n}+2\right)}$$

In general, if other boundary conditions are considered and $d^2v/dx^2\geq 0$, the exact solution is

$$v(x)=\frac{\left[\left(\frac{F\mathbf{1}(x-x_F)}{KI_n}+c_1\right)(x-x_F)+c_1x_F+c_2\right]^{1/n+2}}{\left[\frac{F\mathbf{1}(x-x_F)}{KI_n}+c_1\right]^2\left(\frac{1}{n}+1\right)\left(\frac{1}{n}+2\right)}+c_3x+c_4$$

provided $c_1+F\mathbf{1}(x-x_F)/KI_n\neq 0$ for all $0<x<L$. The constants $\{c_1,c_2,c_3,c_4\}$ can be determined by the boundary conditions.

If further assumes $n=1$ (i.e., the linear beam), then Eq. (7) can be simplified as

$$\frac{d^4v}{dx^4}=\frac{F\delta(x-x_F)}{KI_n},\quad 0<x<L$$

the exact solution for this linear case is simple and can be easily shown as:

$$v(x)=\frac{F\mathbf{1}(x-x_F)}{6KI_n}(x-x_F)^3+c_1x^3+c_2x^2+c_3x+c_4,\quad 0<x<L$$

If $f\neq 0$ (i.e., both constant distributed load and punctual load are considered), the exact solution can be obtained by incorporating the solution in case 1 (for $n=1$) by the additivity property of linearity. It is clear that the analytic solutions derived in this section include the classical solutions of the linear Euler–Bernoulli equation as special cases.

6. Illustrative examples

Numerical examples are provided in this section to demonstrate the applicabilities and performances of our algorithm by comparing it with the analytical solutions derived in the previous section.

6.1. Example 1

In this case, only the constant distributed load f is considered. The parameters are given in Table 1. Assume the two ends of the

Table 1
The parameters of Example 1.

ne	L	$f(x)$	$l^{(e)}$	K	I_n
8	1	1	L/ne	1	$6/[2^n(n+2)]$

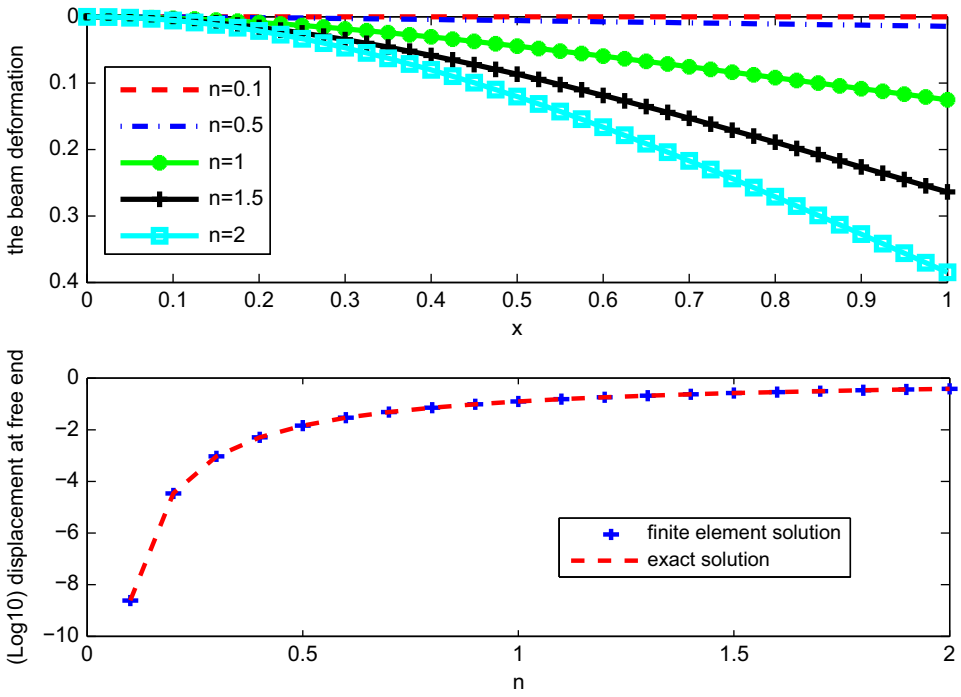

Fig. 1. Example 1. Top figure, the finite element solution of the beam deformation. Bottom figure, the finite element solutions and exact solutions of the displacements at the free-end ($x=L$).

Table 2
The parameters of Example 2.

ne	L	F	$l^{(e)}$	x_F	K	I_n
8	1	3	L/ne	0.5	1	$6/[2^n(n+2)]$

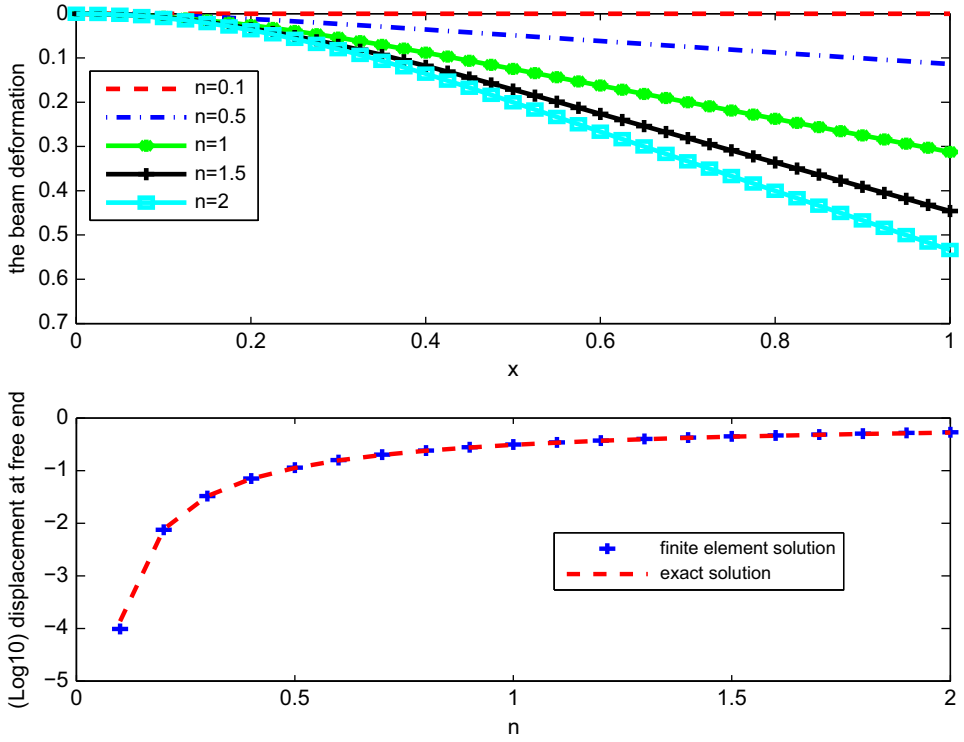

Fig. 2. Example 2. Top figure, the finite element solutions of the beam deformation. Bottom figure, the finite element solutions and exact solutions of the displacements at the free-end ($x=L$).

Table 3
The parameters of Example 3.

ne	L	$f(x)$	$l^{(e)}$	F	x_F	K	I_n
8	1	1	L/ne	-0.4	0.5	1	$6/[2^n(n+2)]$

beam are fixed (at $x=0$) and free (at $x=L$) respectively, then the boundary conditions are specified by

$$v(0)=0, \quad v'(0)=0, \quad v''(L)=0, \quad v'''(L)=0 \tag{21}$$

The solutions are given in Fig. 1. The top figure shows the beam deformation obtained by finite element solutions. Clearly when n increases the beam deformation also increases, which is in line with common sense. The bottom figure shows the free-end displacement of the beam vs. the work-hardening index n. The maximum relative error of the deformation between exact solution and numerical solution is 1.19% (with $n=0.1$). For larger n, the relative errors are significant smaller. Further improvements may be achieved by increasing the number of elements and/or decreasing the error tolerance in the NCG method, while, as expected, these would also increase computational demands significantly.

6.2. Example 2

In this case we consider the punctual load and let $f=0$. The parameters are given in Table 2. The boundary conditions are the same as those in example 1. The beam deformations are shown in Fig. 2, top. The displacements of the free-end are given in Fig. 2, bottom. Similar as in example 1, the maximum relative error is presented at $n=0.1$ with the magnitude 2.86%, and the errors decrease rapidly for larger n.

6.3. Example 3

In this case, we consider both constant distributed load f and punctual load F. The parameters are given in Table 3. Assume both ends of the beam are fixed, so the boundary conditions are specified as:

$$v(0)=0, \quad v'(0)=0, \quad v(L)=0, \quad v'(L)=0$$

The finite element solutions for different n as well as the exact solution for $n=1$ are given in Fig. 3. It is clear that the analytical solution matches the finite element solution for $n=1$.

6.4. Example 4

In this example, we consider a beam subjected to a linear varying distributed load:

$$f(x)=ax+b, \quad 0<x<L$$

The boundary conditions are the same as in example 1. The parameters are given in Table 4. The finite element solutions for different n as well as the exact solution for $n=1$ are given in Fig. 4.

6.5. Example 5

In this example, we consider a more complicated case — a beam subjected to a punctual load

$$F(x)=F\delta(x-x_F)$$

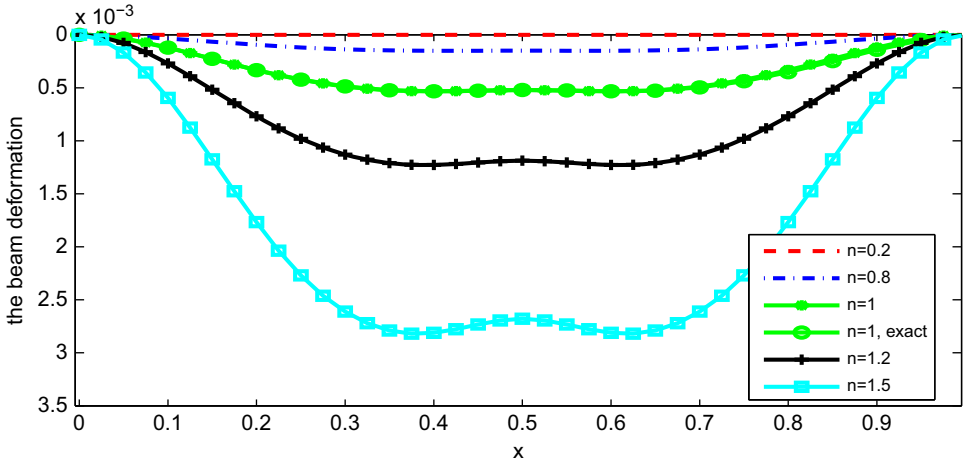

Fig. 3. Example 3. The deformations of the beams subjected to a uniformly distributed load and a punctual load.

Table 4
The parameters of Example 4.

ne	$l^{(e)}$	a	b	L	K	I_n
8	L/ne	3	0	1	1	$6/[2^n(n+2)]$

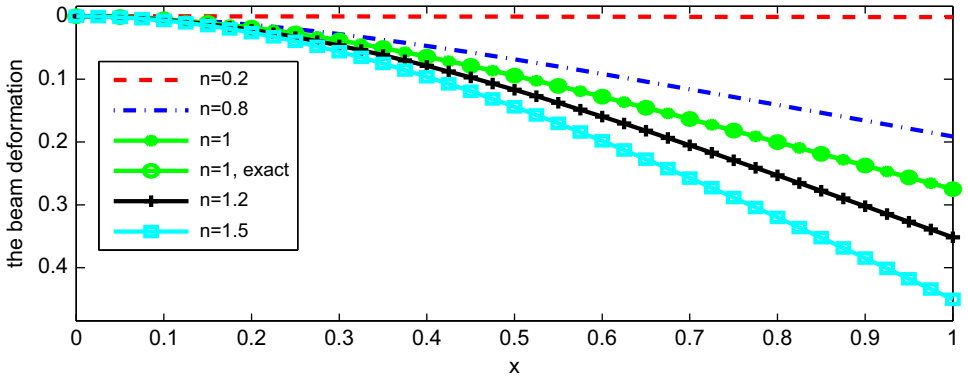

Fig. 4. Example 4, deformations of the beams subjected to linear varying distributed load $f(x)$.

Table 5
The parameters of Example 5.

ne	$l^{(e)}$	L	a	b	f	F	x_F	K	I_n
8	L/ne	1	$0.7L$	$0.9L$	5	-0.25	0.5	1	$6/[2^n(n+2)]$

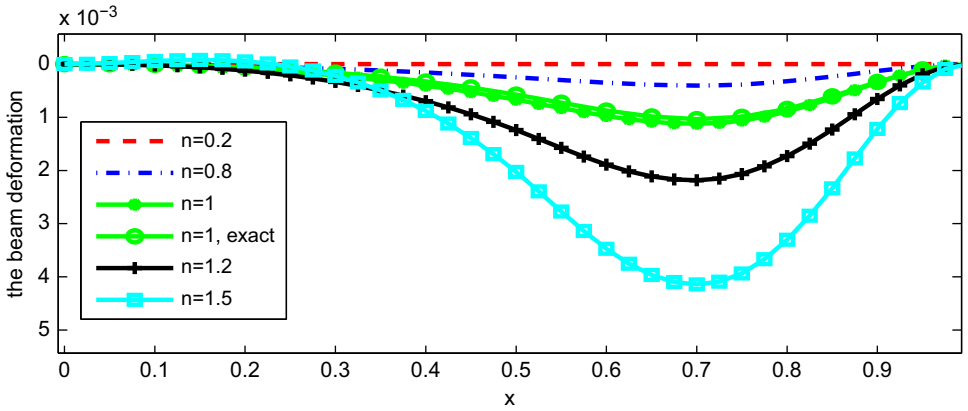

Fig. 5. Example 5, deformations of the beams subjected to a punctual load and a step load.

Table 6
The parameters of Example 6.

ne	$l^{(e)}$	L	c	d	f	K
8	L/ne	1	2	3	1	1

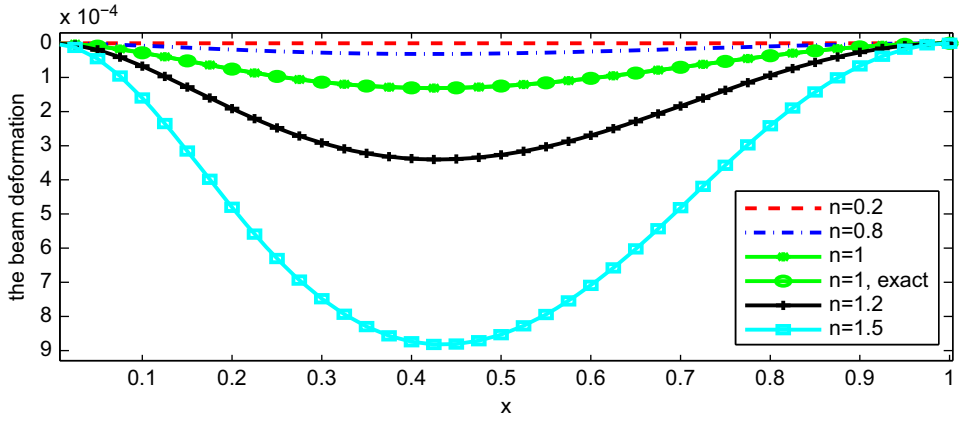

Fig. 6. Example 5, continuous beam.

and a step load within the interval $[a,b] \subset [0,L]$,

$$f(x) = \begin{cases} f, & x \in [a,b] \\ 0 & \text{else } x \end{cases}$$

The parameters are given in Table 5. The numerical solutions as well as the exact solution for $n=1$ are given in Fig. 5.

6.6. Example 6

This example is designed to demonstrate the applicability of our algorithm to the continuous beam, i.e., the cross sectional area $A(x)$ of the beam is varying continuously. We consider a beam with square cross sectional area and its base $h(x)$ of A is varying linearly w.r.t. x, i.e.,

$$h(x) = cx + d, \quad 0 < x < L$$

So it yields

$$I_n(x) = \frac{h(x)^{n+3}}{2^{n+1}(n+2)}, \quad 0 < x < L$$

A uniformly distributed load f is considered and the beam is assumed with two fixed ends. The parameters are given in Table 6. The numerical solutions for different n and the exact solution for $n=1$ are given in Fig. 6. It is observed that the deformations of the beams are not symmetrical w.r.t. $x = L/2$ and lean towards the left. This agrees with common sense because the cross sectional area $A(x)$ is increasing.

7. Conclusions and future work

In this work, we use the Ritz–Galerkin finite element method to approximate the solutions of a nonlinear Euler–Bernoulli beam equation. Hermite cubic finite elements and a nonlinear conjugate gradient scheme are used in the Ritz-finite element method. Convergence and error estimates of the scheme are analyzed.

A finite element code in Matlab is written to implement the scheme. Analytic solutions for some special cases are derived. Numerical solutions provided by the finite element code are compared with the analytic solutions favorably. The results in this work can be extended to the Euler–Bernoulli plate, which is considered as future work.

Acknowledgement

Mr. Juan Gonzalez is gratefully acknowledged for his initial contributions to the Matlab code we developed.

References

[1] J.F. Shackelford, Introduction to Materials Science for Engineers, fifth ed., Prentice-Hall, 2000.
[2] S. Kalpakjian, S.R. Schmid, Manufacturing Processes for Engineering Materials, fourth ed., Prentice Hall, 2002.
[3] Y. Liu, D. Xu, J. Xu, Updated 5-parameters Barlat–Lian yield criteria, J. Huazhong Univ. Sci. Technol. 36 (2008) 129–132. (Natural Science Edition).
[4] T. Dutton, R. Edwards, A. Blowey, Tool design for a high strength steel side impact beam with springback compensation, in: Proceedings of 5th European LS-DYNA Users Conference, 2005.
[5] H. Zhang, Y. Bellouard, E. Burdet, R. Clavel, A.-N. Poo, D.W. Hutmacher, Shape memory alloy microgripper for robotic microassembly of tissue engineering scaffolds, in: Proceedings of the 2004 IEEE International Conference on Robotics & Automation, 2004.
[6] W. Wang, Y. Huang, K.J. Hsia, K.X. Hu, A. Chandra, A study of the microbend test by strain gradient plasticity, Int. J. Plasticity 19 (2003) 364–382.
[7] Y.-A. Kang, X.-F. Li, Bending of functionally graded cantilever beam with power-law non-linearity subjected to an end force, Int. J. Non-Linear Mech. 44 (2009) 696–703.
[8] J. Bin, C. Wanji, A new analytical solution of pure bending beam in couple stress elasto-plasticity: theory and applications, Int. J. Solids Struct. 47 (2010) 779–785.
[9] J. Reddy, Introduction to the Finite Element Method, McGraw Hill, 2006.
[10] J.N. Reddy, Nonlinear Finite Element Analysis, Oxford University Press, 2007.
[11] X. Teng, T. Wierzbicki, Crush response of an inclined beam-column, Thin-Walled Structures 41 (2003) 1129–1158.
[12] H. Yahoobi, A. Feraidoon, Influence of neutral surface position on deflection of functionally graded beam under uniformly distributed load, World Appl. Sci. J. 10 (2010) 337–341.
[13] E.K.P. Chong, S.H. Zak, An Introduction to Optimization, Wiley-Interscience, 2001.
[14] D. Wei, Nonlinear wave equations arising in modeling of some strain-hardening structures, in: Proceedings of Joint Conference of the 6th International Conference of Computational Physics and Conference of Computational Physics, 2005, pp. 248–251.
[15] O. Axelsson, V. Barker, Finite Element Solution of Boundary Value Problems, Academic Press, Inc., Orlando, Flordia, 1984.

[16] M. Abramowitz, I.A. Stegun, Handbook of Mathematical Functions: with Formulas, Graphs, and Mathematical Tables, Dover Publications, 1964.
[17] E. DiBenedett, Degenerate Parabolic Equations, Springer-Verlag, 1993.
[18] R. Glowinski, A. Marrocco, Sur l'approximation par éléments finis et la résolution, par pénalisation-dualité, d'une classe de problèmes de Dirichlet non linéaires, Rev. Fr. d'Autom. Inf. Rech. Oper. Sér. Rouge (Analyse Numérique) R-2 (1975) 41–76.
[19] J.W. Barrett, W.B. Liu, Finite element approximation of the *p*-Laplacian, Math. Comput. 61 (1993) 523–537.
[20] M.S. Bazaraa, H.D. Sherali, C.M. Shetty, Nonlinear Programming—Theory and Algorithms, third ed., John Wiley & Sons, Inc., Hoboken, New Jersey, 2006.
[21] H. Liu, S.S. Cheng, X. Li, A conjugate gradient method with sufficient descent and global convergence for unconstrained nonlinear optimization, Appl. Math. E-Notes 11 (2011) 139–147.
[22] A.B.O. Daalhuis, Hypergeometric function, in: F.W.J. Olver, D.M. Lozier, R.F. Boisvert, et al. (Eds.), NIST Handbook of Mathematical Functions, Cambridge University Press, 2010.
[23] R.K. Nagle, E.B. Saff, A.D. Snider, Fundamentals of Differential Equations, fifth ed., Addison Wesley Longman Inc, 2000.